We are IntechOpen, the world's leading publisher of Open Access books Built by scientists, for scientists

4,800
Open access books available

122,000
International authors and editors

135M
Downloads

Our authors are among the

154
Countries delivered to

TOP 1%
most cited scientists

12.2%
Contributors from top 500 universities

WEB OF SCIENCE™

Selection of our books indexed in the Book Citation Index in Web of Science™ Core Collection (BKCI)

Interested in publishing with us?
Contact book.department@intechopen.com

Numbers displayed above are based on latest data collected.
For more information visit www.intechopen.com

Chapter 7

Fracture Behavior Evaluation of High-Strength 7050 and 7075 Aluminum Alloys Using V-Notched Specimen

Parvin Abachi, Pouyan Shoushtari Zadeh Naseri, Kazem Purazrang and Tom W. Coyle

Additional information is available at the end of the chapter

http://dx.doi.org/10.5772/64463

Abstract

The fracture behaviors of high-strength 7050 and 7075 aluminum alloys (AA7050 and AA7075) were investigated using small size, V-notched tear specimens. In accordance with ASTM B871-01 standard test method, the thickness and notch angle were selected as 6.35 mm and 60°, respectively. All tear specimens (also called Kahn specimens) were machined in L-T orientation and the mechanical tests were conducted at RT. To evaluate crack propagation route during failure process, interrupted tear tests were also conducted on AA7075. The subsized cylindrical tension test specimens were machined in L direction of the bulk materials to study the elastic-plastic behavior of the alloys in accordance with ASTM B 557M-98 standard test method. The microstructures of T73651 and T6 heat-treated alloys were examined using optical microscopy and SEM. The precipitate characterization of heat-treated specimens was performed using Clemex image analysis software. The rupture mechanisms were also studied by examination of specimen fracture surfaces using SEM. According to the results, the amount, size and distribution of intermetallic particles have been identified as the important factors on failure of the examined alloys. Both examined alloys show the same damage initiation mechanism; however, the failure mechanism is different to some extent. Depending on the stress condition, two major failure micromechanisms, i.e., "internal necking mechanism" and "void sheet mechanism," are prevailing for both alloys. The results of mechanical tests and determination of tear strength to 0.2% tensile yield strength ratio made it possible to evaluate specimens' notch toughness. The comparison of specimens' resistance to stable crack propagation and subsequent fracture in the presence of crack-like stress concentrator was provided using tear test data.

Keywords: aluminum alloys, V-notched tear specimen, microstructure, precipitates, notch toughness

1. Introduction

In aerospace industry, wings-, tail-leading edges and fuselage materials require high crack initiation and propagation resistance under applied loads. In design consideration, the material should be identified and examined to provide service requirements such as high specific strength, fatigue resistance, fracture toughness, high crack initiation and propagation energies, reproducibility, reliability and safety. Aluminum alloys of the 7xxx series (Al-Zn-Mg-Cu alloys) show an exceptional combination of static tensile properties, failure resistance and good machine-ability. On this account, they are used exceedingly in aerospace industry, particularly in upper and lower wing skins in some planes [1–4]. AA7050 guarantees the same resistance to stress corrosion and exfoliation corrosion at higher strength levels compared to AA7075 [5]. Typical applications of AA7050 plates are in fuselage frames and bulkheads, while AA7050 sheets are used for wing skins. AA7050 is also used to produce extrusions, forgings and fasteners. Examples of application of 7xxx aluminum alloys in the aerospace industry are presented in **Figure 1** [5]. Higher Zn and Cu contents in alloy 7050, in comparison with alloy 7075, compensate the strength loss caused by over aging to T7 condition in order to improve stress corrosion resistance as well as fatigue crack propagation resistance. "Replacement of Cr by Zr makes the alloy less quench sensitive. The ability to be quenched at a reduced rate while retaining adequate strength is an asset for an alloy intended to be used in heavy sections where thermal conductivity limits quench rate or to be quenched at slower rate to minimize thermal stresses" [6]. Reduction of Fe and Si improves fracture toughness.

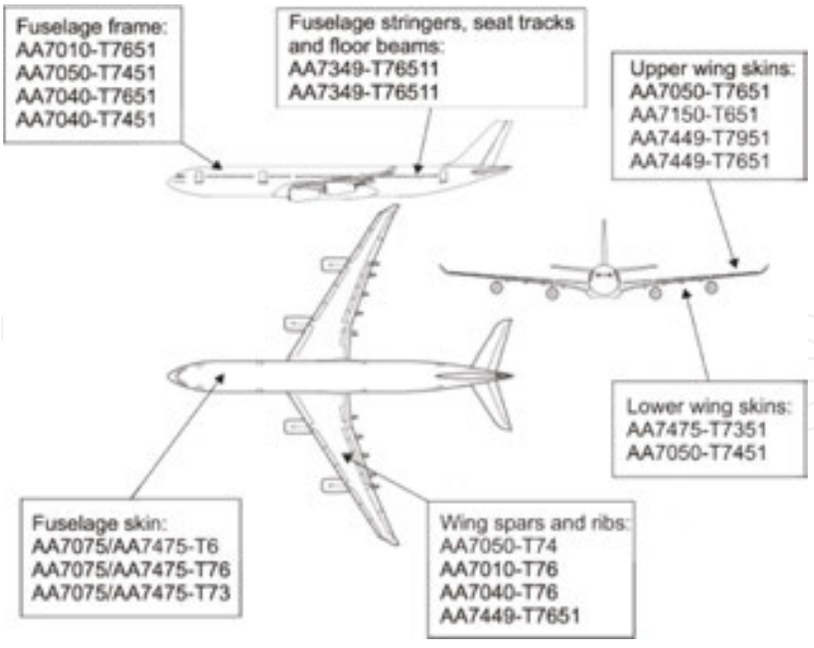

Figure 1. Examples of application of 7xxx aluminum alloys in the aerospace industry (adapted from [5]).

As mentioned above, wing and fuselage materials are expected to show high resistance against development and propagation of cracks initiated under normal load spectrums [7, 8]. There-

http://dx.doi.org/10.5772/64463

fore, among all the property requirements, the fracture toughness is often the limiting design consideration [7, 9].

There are various testing methods to determine material toughness. Designers may apply ductile crack growth resistance test, referred to as R-curve test conducted on either the middle-cracked tension (MT) or the compact tension (CT) specimen, or the crack line wedge loaded (CW) specimen, according to the ASTM E561-86 standard [10]. Another standard test is also suggested for fracture toughness testing of aluminum alloys [11]. Of all the above methods, the plane strain compact tension test CT is considered to be one of the most accurate methods to measure K_{IC} [12]. However, CT specimens are costly and time consuming to construct. Moreover, it is difficult to obtain valid K_{IC} with respect to test specifications [10, 13]. Small-size specimens, i.e., tear specimens, the so-called "Kahn specimens,"[1] provide several numerical results such as unit initiation and propagation energies, tear strength, notch toughness or TYR (tear strength to 0.2% yield strength ratio) [7, 13–15]. In the tear test, a V-notched specimen with the notch radius less than 60 μm is subjected to static tensile loading until a crack develops at the root of the notch and passes through the width of the specimen [13, 14]. Such specimens have superior advantages as low cost, short time of preparation and low material consumption. In addition, no fatigue precrack is required and the sharp notch (V-notch having root radius less than 60 μm) acts as a stress concentrator and, therefore, it may replace to others requiring fatigue precrack. According to the work results of Bron et al. [7] on two grades of 2024 aluminum alloys, similarity of fracture surfaces and identical failure mechanics in Kahn specimens and precracked large middle-cracked tension M(T) panels make it possible to predict the cracking behavior of large M(T) as well as actual structures using experimental results on small ones.

The extraordinary combination of properties in 7xxx series of aluminum alloys as mentioned above is attributed to the proper microstructures obtained by the aging processes, which is applicable due to the presence of different alloying elements in the alloy composition [3, 15]. The microstructure of heat-treated specimens could contain coherent, semicoherent and even incoherent precipitates which affect the physical and mechanical properties. Many investigations have been performed on the microstructure evolution during aging of 7xxx Al alloys [16–20] and some research works have been conducted to study the relationship between aging patterns and mechanical properties [21–27]. Deshpande et al. [24] have studied the evolution of toughness with aging time in AA7050. Dumont et al. [26] have also investigated the influence of the microstructure on strength and toughness in AA7050 aluminum alloy. Srivatsan [27] has evaluated the influence of the microstructure on fatigue and fracture behavior of the aged AA7050 alloy. The multistage aging heat treatment contributes to better distribution of precipitates and is also consistent with industrial practice [21, 26]. Moreover, secondary aging at elevated temperatures provides microstructure stability, i.e., mechanical properties of an age-hardened alloy remain unchanged for an indefinite period if used in service at close to the ambient temperature. Referring to Lumley et al. [28], multistage heat treatments, like T73 temper, provide a means for improving the properties of aged aluminum alloys by modifying

[1] N.A. Kahn has firstly used a very sharp notch, in place of the key-hole notch, in samples to facilitate the crack initiation at relatively low energy levels and increase the ability to measure accurately the required crack propagation energy.

the size, composition, species and distribution of precipitate particles. Additionally, the T73 temper increases the stress-corrosion resistance of 7xxx series (Al-Zn-Mg-Cu) wrought alloys by modifying the microstructure. However, there is a significant sacrifice in tensile properties, compared with the single-stage T6 temper. Considering Dungore and Agnihotri [29] statements, by application of various tempers such as T73, T76 and T39, it is possible to overcome some drawbacks of high-strength heat-treatable aluminum alloys like reduced ductility and fracture toughness in the short transverse direction and enhanced stress corrosion cracking (SCC) susceptibility. T73 temper is used to improve the corrosion resistance. However, referring to Kumar et al. [30] work results, the post weld heat treatment of AA7075 alloys at overaged (T73) temper is accompanied with a loss of strength about 10–15% compared to T6 temper. Therefore, retrogression and re-aging (RRA) treatment can be used as an alternative treatment to recover the strength of 7xxx series alloys without impairing the corrosion resistance of the material. Post weld treatment to RRA leads to the dissolution of the less stable precipitates (GP zones and η′) inside the grains and the increase of grain boundary precipitates (GBPs). In this work, the fracture behavior of two popular 7xxx series aluminum alloys, i.e., AA7050 and AA7075, was examined after multistage and single-stage precipitation hardening (age hardening) heat treatments and the fracture mechanisms of smooth and notched specimens were compared.

2. Experimental

Two types of high-strength aluminum alloys of 7xxx series, i.e., AA7075 and AA7050, were provided for this investigation. The chemical compositions of test materials in weight percent are presented in **Table 1**. The dimensions of provided plates were 200 cm×100 cm×11 cm in the case of cold rolled AA7050 and 60 cm×10 cm×7 cm for extruded AA7075. Since overaging T7 temper provides the best resistance to exfoliation corrosion and SCC as well as enhancement of fatigue crack growth resistance, the multistage T73651 temper is suggested for AA7050. In addition, this aging treatment contributes to dimensional and thermal stability of the part besides better distribution of precipitates. It is also consistent with industrial practice. Therefore, multistage T73651 temper which was applied to AA7050 by manufacturer [31] consisted of the solid solution treatment (homogenization) at 477°C, followed by quenching at warm (65°C) water and finally two aging stages. The initial artificial aging was performed at 120°C for 24 hours and the final artificial aging at 163°C for the same period of time. Alternatively, the AA7075 alloy, after 1-hour solution treatment at 468°C, was quenched in water to room temperature. This was followed by artificial aging at 120°C for 24 hours. It can be considered as T6 heat treatment.

Metallographic specimens were prepared, polished and etched in Keller's solution for 10–18 seconds [32]. The microstructures of specimens were examined using optical microscopy and SEM. The Brinell hardness measurement was performed with 62.5 kg load using steel ball with 2.5 mm diameter in different orientations. The subsized cylindrical tension test specimens were machined in L direction of the bulk materials to study the elastic-plastic behavior of the alloys

http://dx.doi.org/10.5772/64463

in accordance with ASTM B 557M-98 standard test method [33]. The tests were carried out on a House field H 10 KS testing machine with crosshead speed of 0.5 mm/min.

Alloy	Elements									
	Zn	Mg	Cu	Mn	Cr	Si	Fe	Zr	Ti	Al
AA7050	5.7–6.7	1.9–2.6	2.0–2.6	0.1 max	0.04 max	0.12 max	0.15 max	0.08–0.15	0.06 max	Balance
AA7075	5.1	1.8	1.24	1.65	0.25	0.61	0.18	<0.1	<0.1	Balance

Table 1. The chemical compositions of AA7050 and AA7075 in wt.%.

All tear specimens were machined in L-T orientation and the mechanical tests were conducted at RT on a Universal Instron-6027 tension testing machine with especially low crosshead speed of 0.1 mm/min up to the fracture point. A displacement gauge was attached to the fixtures to monitor the displacement values. For crack route detection, interrupted tear tests were also performed on AA7075. For this purpose, four specimens were tested. For each specimen, the test was interrupted in a specific point (load). The crack route was detected by penetration of ink into the crack area before final specimen rupture. The V-notched specimens with 6.35 mm thickness, 36.5 mm width and 57.15 mm length are shown schematically in **Figure 2a**. The L-T orientation, which corresponds to the loading of specimens in L direction and the crack propagation in T direction, is presented in **Figure 2b**. In this designation L and T represent rolling and long transverse direction, respectively. It has been reported that when the specimens are loaded in rolling direction, resistance against crack propagation increases. This is contributed to formation of larger shear lips and therefore higher fracture toughness [34]. Varli and Gürbüz [35] have pointed out that 6013 aluminum alloy exhibits the highest resistance to fatigue crack growth in the L-T orientation. The notch root angle was selected as 60°, in accordance with ASTM B871-01 standard test method for tear testing of aluminum alloy products [14]. The root radii of sharp V-notches, which act as a stress concentrator, were selected as 20 and 60 μm.

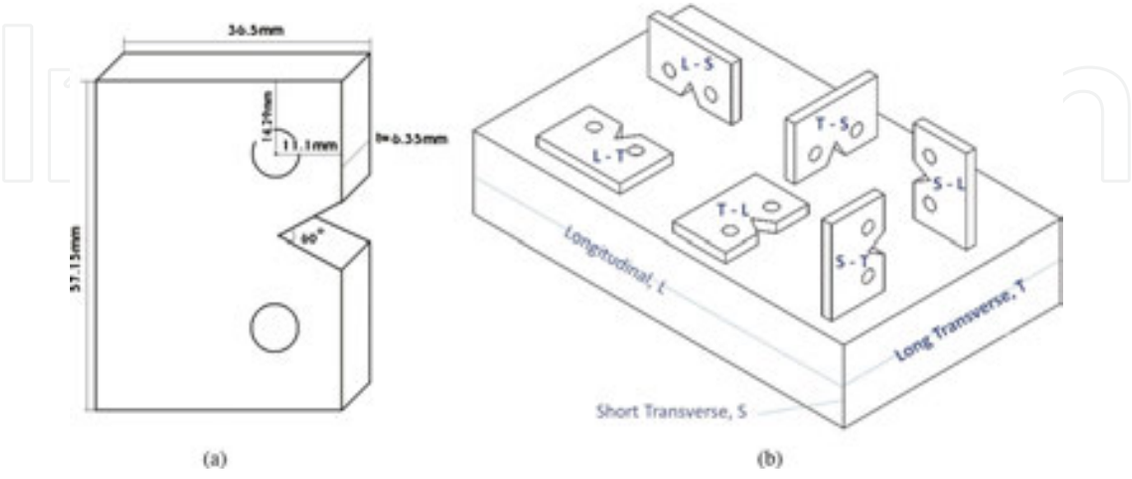

Figure 2. (a) The geometry and dimensions of tear test specimen and (b) location of tear test specimens in different orientations (L = longitudinal rolling direction, T = long transverse direction and S = short transverse direction).

3. Results and discussion

3.1. Microstructure

The microstructures of AA7050 and AA7075 alloys in L-T orientation are shown in **Figure 3**. The microstructures mainly consist of equiaxed grains and some elongated grains in rolling or extrusion direction, with the areas of partial recrystallized grains where coarse intermetallic (IM) particles are mostly found. In L-T orientation, average grain area is 10×4 μm^2 in AA7050 and 45×12 μm^2 in AA7075. The presence of coarse intermetallic particles in recrystallized grains location suggests that the recrystallization has occurred mainly with particle stimulated nucleation (PSN) mechanism which is also stated by other researchers [15, 20, 36–38]. However, small precipitates (particularly Al_3Zr) in some areas have prohibited the recrystallization to develop. Deshpande et al. [24] have also mentioned that presence of Zr in AA7050 leads to formation of the Al_3Zr dispersoids which retard the recrystallization process. Cvijović et al. [39], in studies on microstructural dependence of fracture toughness in high-strength 7xxx forging alloys, have also pointed out to the unrecrystallized grain structure due to appreciable amounts of Cr, Mn and Zr which are known to be efficient in the formation of dispersoids as recrystallization inhibitors. It is stated that, in 7075 aluminum alloy, $Al_{12}Mg_2Cr$ is a common dispersoid [40]. The voids of both alloys, which are evident on micrographs in BS mood, are presented in **Figure 4**. In these micrographs, precipitates are appeared white, voids black and the matrix gray. The density of voids was determined 0.9 and 1.7% in AA7050 and AA7075, correspondingly. Regarding the less amounts of voids in comparison to precipitates, they may have far less important role in crack initiation process. Nevertheless, there is also a possibility for partly void formation in the polishing practice. In general, microstructural features affect some mechanical properties of 7xxx series alloys such as strength, fracture toughness as well as corrosion resistance. Therefore, the properties of the heat-treated 7xxx series aluminum alloys depend on grain size, void content, as well as dispersoids, intermetallic (IM) compounds, constituent particles, the matrix precipitates (MPs), grain boundary precipitates (GBPs) and precipitate-free zones (PFZs) [41]. According to the selected optimized process of heat treatment, the combined properties can be obtained by the cooperation of the above-mentioned microstructural features. The microstructures of two popular 7xxx series aluminum alloys, i.e., AA7050 and AA7075, after multistage T73651 and single-stage T6 precipitation hardening (age hardening) heat treatments include fine and coarse precipitates which are evident on the as-polished micrographs in **Figure 5**. The results of EDAX studies on fracture surfaces, which have been reported elsewhere [42], showed that besides stable phase ($MgZn_2$), the coarse intermetallic particles can be Al_7Cu_2Fe, Al(Fe,Mn)Si, Al_2CuMg and Al_2Cu, Mg_2Si, Al_2CuMg in AA7050 and AA7075, respectively. Xie et al. [16] have found Sigma (Al,-Cu,$Zn)_2Mg$, S (Al_2MgCu), θ (Al_2Cu), Mg_2Si, Al_7Cu_2Fe and $Al_{13}Fe_4$ in the structure of solidified aluminum 7050 alloy. According to Srivatsan [26] work, the intermediate η′ ($MgZn_2$) precipitate is the most important strengthening phase in age hardenable Al-Zn-Mg 7xxx series alloys, whereas the β′ (Al_3Zr) dispersoids (f.c.c.-based L1 structure) appear due to the presence of the grain-refining element zirconium, hinders the recrystallization. According to SEM/EDS

http://dx.doi.org/10.5772/64463

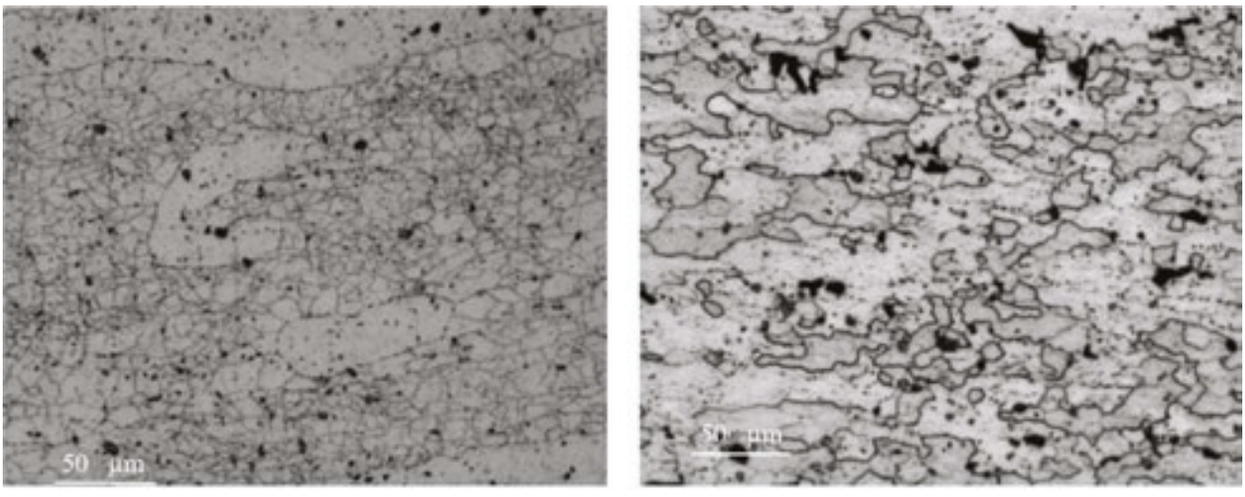

Figure 3. Optical micrographs of (a) AA7050 and (b) AA7075.

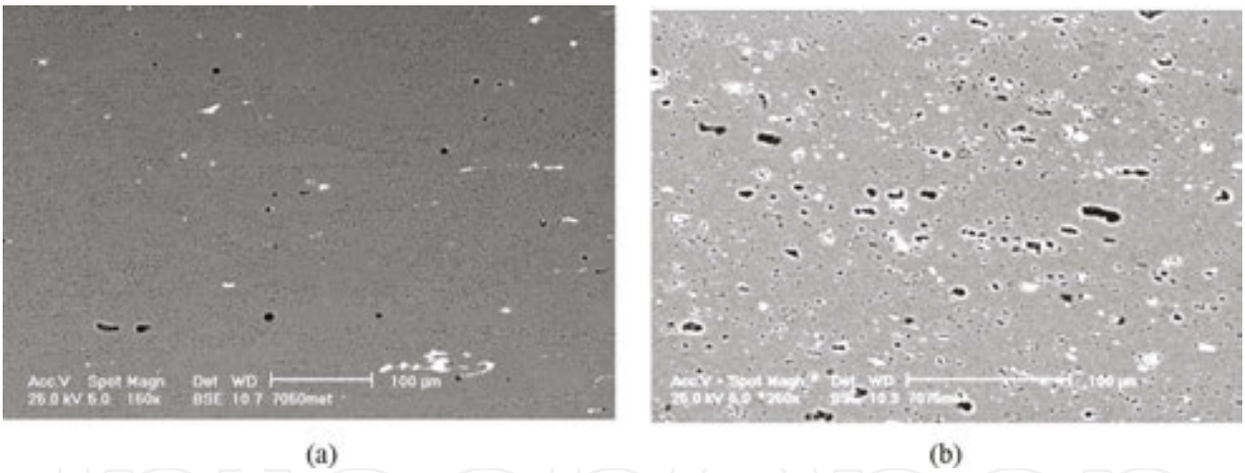

Figure 4. SEM micrographs revealing the presence of voids in (a) AA7050 and (b) AA7075 in BS mood.

studies of Cvijović et al. [39] on overaged 7000 alloy forgings, the coarse IM particles, aligned in the direction of prevailing deformation, are η-$Mg(Zn,Cu,Al)_2$, S-Al_2CuMg associated with Zn, Mg_2Si (as soluble IMs) and $Al_3(Cu, Fe,Mn)$, Al_7Cu_2Fe, plus a little of $Al_7(Cu, Fe,Mn,Cr)$ (as insoluble IMs). Andreatta [5] has also concluded that the most abundant intermetallics in AA7075 are the Cu- and Fe-rich intermetallics such as Al_7Cu_2Fe and $(Al,Cu)_6(Fe,Cu)$, while the Mg_2Si intermetallic is present in smaller quantity.

In **Figure 6**, image analysis results related to precipitate size distribution are shown. The dimensions and shape factors of the precipitates, which are determined by Clemex image analysis software, are also presented in **Table 2**.

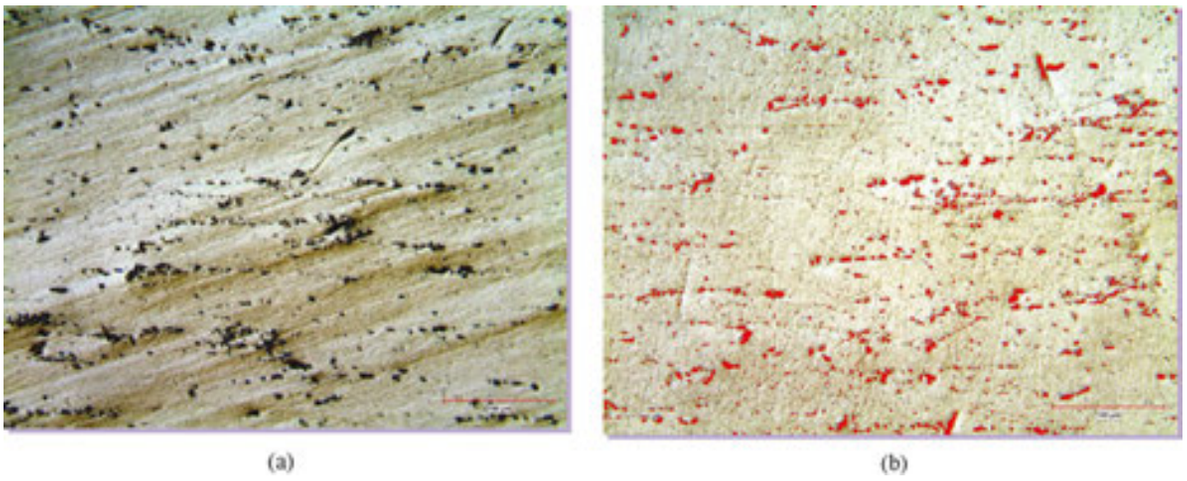

Figure 5. The microstructure of (a) AA7050 and (b) AA7075 in polished condition.

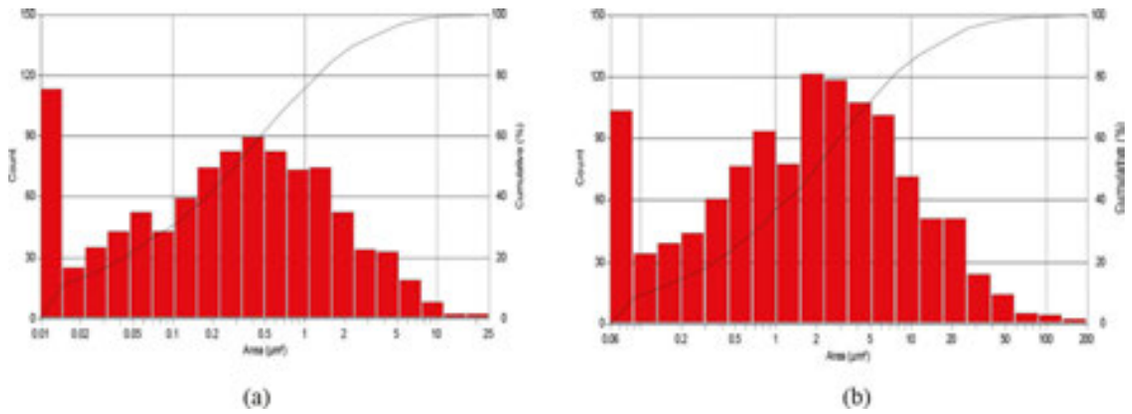

Figure 6. The size distribution of precipitates in (a) AA7050 and (b) AA7075.

Referring to Pao et al. [43], the formation of coarse precipitates at grain boundaries, due to the ready diffusion of solute atoms into the boundary, depletes the solid solution in their immediate surroundings. This leads to creation of a precipitate-free zone (PFZ). Moreover, depletion of vacancies to levels below that needed to assist with nucleation of precipitates at the particular aging temperature should be also considered as a reason for PFZ formation [44].

Occurrence of intermetallic particles in the grain and subgrain boundaries would result in low mechanical properties and resistance to fracture for two main reasons: firstly, these particles are the appropriate sites for crack initiation within the microstructure and secondly, the formation of coarse precipitates will create precipitate-free zone at both sides of grain boundary. PFZs are regions with low strength and so preferred areas for crack propagation. According to the work of Cai et al. [45] on AA7050 alloy, the precipitation-free zone (PFZ) is very narrow for double-step hot rolling (DHR)-treated alloy, which is beneficial to the mechanical properties. According to Polmear [44] statements, for higher solution treatment temperatures, faster quenching rates (both of which increase the excess vacancy content) and lower aging temperatures, the PFZs are narrower. However, continuous GBPs and narrow PFZ

http://dx.doi.org/10.5772/64463

increase the SCC susceptibility of the alloy (e.g., in T6 condition) and the discrete GBP and wide PFZ (e.g., attaining after RRA treatment consisting of pre-aging, retrogression and re-aging) can improve the SCC resistance of the alloy and decrease its SCC index [41].

Alloy	Specifications					
	Precipitate content (%)	Max. length (μm)	Min. length (μm)	Ave. length (μm)	Roundness	Aspect ratio
AA7050	2.9	9.8	0.12	1.24	0.81	1.75
AA7075	3.5	28.6	0.25	2.35	0.79	1.76

Table 2. The dimensions and shape factors of precipitates detected in L-T plane of AA7050 and AA7075 alloys.

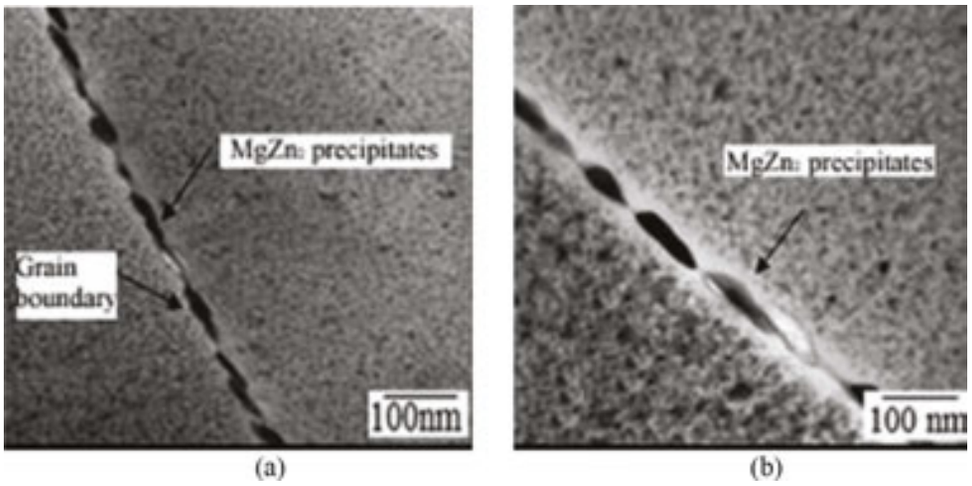

Figure 7. Showing (a) continuous GBPs plus narrow PFZ in AA 7075 alloy in T6 condition and (b) the discrete GBPs plus wide PFZ after RRA treatment (adapted from [29]).

Referring to Ranganatha et al. [46], by retrogression and re-aging (RRA) heat treatment, the resistance to SCC is enhanced without losing yield or tensile strength. "The longer retrogression time during the RRA treatment leads to a combination of grain boundary η precipitate coarsening, which resembles the precipitates formed in the T73 temper and the η-η′ precipitates distribution in the matrix which looks like the precipitates formed in the T6 temper. This combination results in good performance with respect to resistance to stress corrosion cracking and the thermodynamic stability as well as mechanical strength" [46]. The TEM study results of Kumar et al. [30] on AA7075 in different heat treatment conditions show the dispersion of precipitates η′ and η in the alloy matrix along with coexistent coarser and sparsely distributed η precipitates locating at the grain boundaries, together with precipitate-free zones (PFZs), **Figure 7**. Goswami et al. [47] have related the SSC resistance to the increase in Cu content of the $Mg(Cu_xZn_{1-x})_2$ precipitates at grain boundaries and, therefore, depletion of both zinc and copper in the PFZ relative to the matrix, in the overaged (T73) and RRA conditions. "The electrochemical potential of the intermetallic $Mg(Cu_xZn_{1-x})_2$ compound increases with the increase in Cu content. This decreases the driving force for anodic dissolution with respect to

matrix, particularly for the overaged condition where the Cu level is highest. As the dissolution rate decreases with increasing Cu content, the alloy becomes less susceptible to SCC" [47].

In the present work, application of two different precipitation hardening heat treatments can also affect the mechanical properties, due to the above-mentioned reasons.

3.2. Hardness measurements and tension test results

The results of hardness measurements and tension tests of both alloys are given in **Tables 3** and **4**. Considering the results of hardness testing, it is believed that the formation of texture has a little effect on hardness and, therefore, the slightly higher hardness value in S-T orientation can be due to higher density of grain boundaries and the fact that precipitation ensues preferably in these areas.

Alloy	**Hardness HB (kgf/mm²)**		
	L-T plane	**S-T plane**	**L-S plane**
AA7050	151.5	155.1	150.0
AA7075	165.4	169.6	167.8

Table 3. The average Brinell hardness values of AA7050 and AA7075 in different orientations.

Alloy	**Property**			
	UTS (MPa)	**$\sigma_{0.2}$ (MPa)**	**E (GPa)**	**ε_f (%)**
AA7050	606	430	86.2	23.06
AA7075	582	406	62.8	22.98

Table 4. The average tensile properties values of AA7050 and AA7075 in L direction.

In respect of tension tests which were performed on the cylindrical specimens in L direction, it emerges that the elastic-plastic behaviors of both alloys are almost alike and slightly better strength of AA7050 may be attributed to the effects of the finer grains, low preliminary void content. However, large interparticle spacing and wide PFZs in the T73 temper could be unfavorable to the strength of material. Sarkar et al. [48] studies on AA5754 showed that when interparticle spacing is fairly large, the alloy fails in a typical cup and cone mode (ductile failure). However, the small interparticle spacing promotes linking of voids associated with coarse particles and leads to failure by void sheeting.

3.3. Tear test results

After applying the static tensile load on tear test specimen, a crack develops at the root of notch and travels across the width of the specimen. The study on AA7050 and AA7075 shows that two different forms of load-displacement curves can be achieved as a result of a tear test. In

http://dx.doi.org/10.5772/64463

the first one that we denote the specimen as "A" in this article, after maximum value of load, there is a large spontaneous decrease in sustained load. This phenomenon was referred to as "Pop In" in some other articles [13, 49]. In this situation a crack initiates at the point of maximum load. In other curves, referred to specimen as "B", the load decreases smoothly, after its maximum point and the crack initiation occurs somewhat before the maximum load. This occurrence has also been reported in the case of specimens with thickness of less than 5 mm [13, 49]. Nevertheless, in this study, the only variable is the specimen notch root radius (NRR) value which leads to this diversity. In the case of type "A", NRR is about 20 μm while in "B" it equals to 60 μm. So, it can be concluded that the effect of the NRR decrease is quite similar to the increase in thickness which leads to plane strain condition prevailing [13]. **Figures 8** and **9** illustrate load-displacement curves as primary results of tear tests performed on type "A" and "B" specimens in both aluminum alloys. In **Table 5**, the related results such as tear strength, notch toughness initiation energy (IE) and propagation energy (PE) are presented for both alloys.

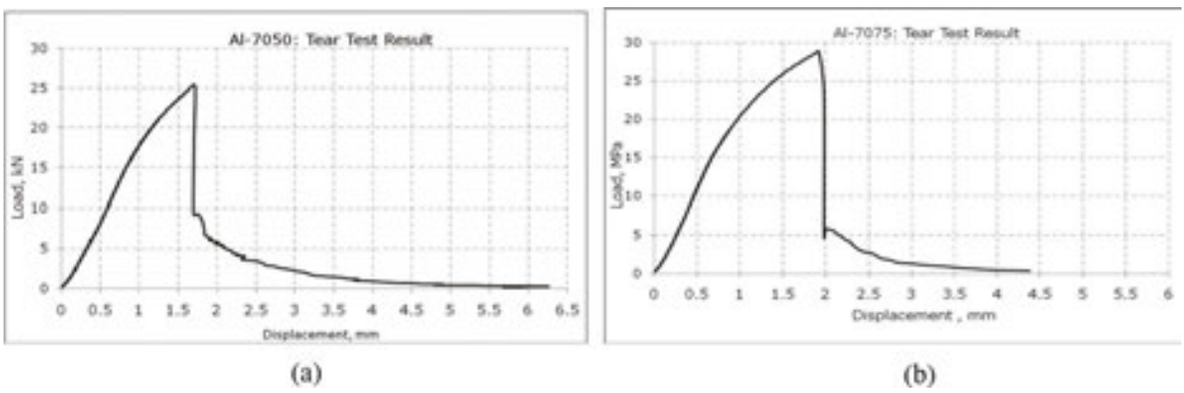

Figure 8. Load-displacement curves as primary results of tear tests performed on type "A" specimens of (a) AA7050 and (b) AA7075.

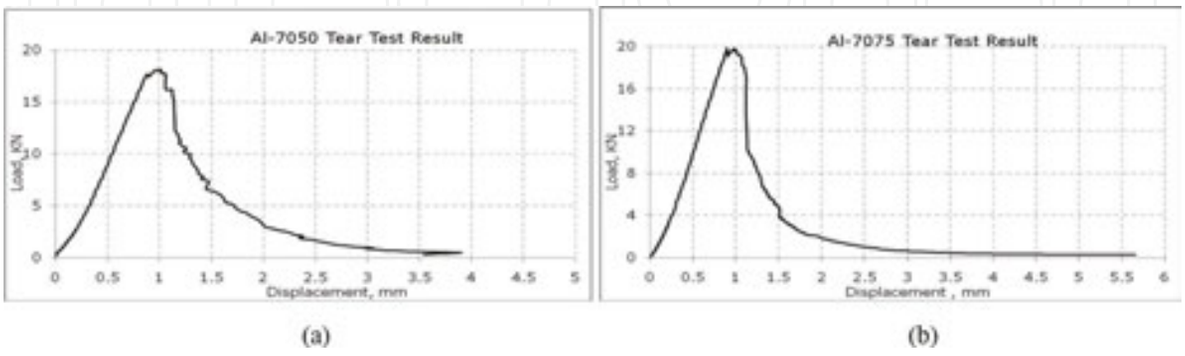

Figure 9. Load-displacement curves as primary results of tear tests performed on type "B" specimens of (a) AA7050 and (b) AA7075.

Alloy	Property							
	Specimen designation	NRR (μm)	Tear strength (MPa)	Notch[1] toughness	IE[2] (N.m)	PE[3] (N.m)	UIE[4] (kN/m)	UPE[5] (kN/m)
AA7050	A	20	628.20	1.46	24.30	8.00	150.70	50.10
AA7050	B	60	449.84	1.05	6.74	11.56	41.80	72.27
AA7075	A	20	716.50	1.76	33.80	4.10	209.40	25.90
AA7075	B	60	531.66	1.32	7.93	10.58	49.20	65.63

[1]Tear strength/$\sigma_{0.2}$ (notch toughness).
[2]Crack initiation energy.
[3]Crack propagation energy.
[4]Unit initiation energy.
[5]Unit propagation energy.

Table 5. The tear test results of AA7050 and AA7075 specimens, containing different NRRs, in L-T orientation.

It can be noticed that for both types of curves in **Figures 8** and **9**, the maximum load values of AA7075 are higher than those of AA7050 alloy which consequently lead to the occurrence of higher notch strengths. This could be considered as a direct result of higher content of precipitates in this alloy and probably narrower PFZs. Clearly, the lower $\sigma_{0.2}$ yield strength of AA7075 could be related to coarser grains and higher primary void content. Additionally, these curves show that crack initiation energy (IE) of AA7050 is lower than that of AA7075 regardless of specimen type ("A" or "B"). In contrary, the crack propagation energy (PE) is higher for AA7050 which can be due to slanted or blunted crack tip in this alloy. Obviously, the large precipitates can be considered as nucleation sites for voids in the crack initiation stage as well as void growth and coalescence sites during crack propagation process.

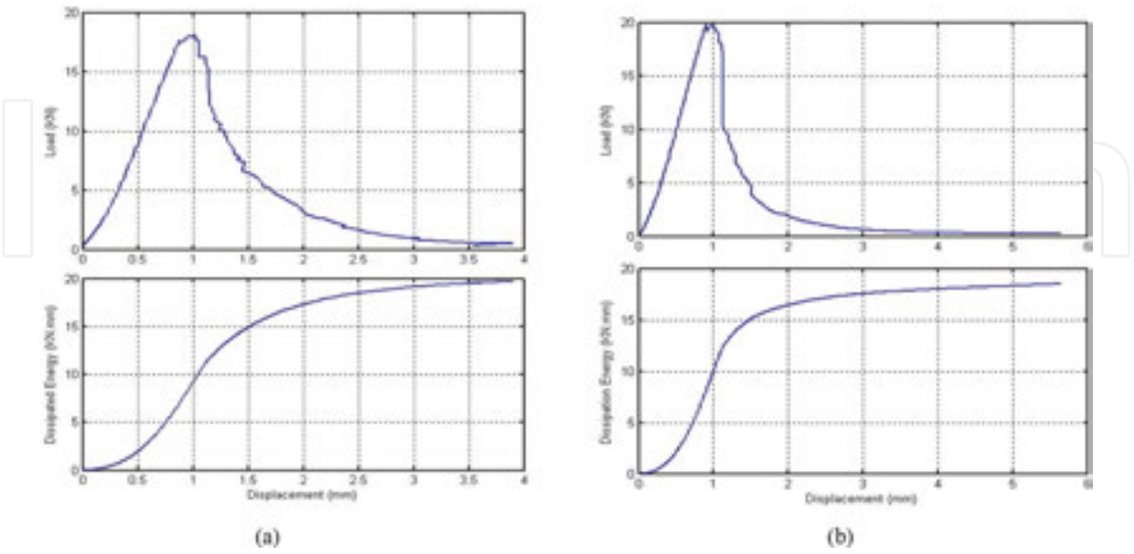

Figure 10. Load-displacement and energy dissipation curves for type "B" tear specimens of (a) AA7050 and (b) AA7075.

http://dx.doi.org/10.5772/64463

In **Figure 10**, the amount of dissipated energies during failure process for type "B" tear specimens is shown. The slopes of these curves represent the energy dissipation rates during rupture process. The maximum of dissipation rate in both alloys belongs to crack initiation stage and minimum to crack propagation stage. Furthermore, in AA7050, the energy dissipation rate exceeds that of AA7075 in crack propagation stage and reverse situation exists in crack initiation stage.

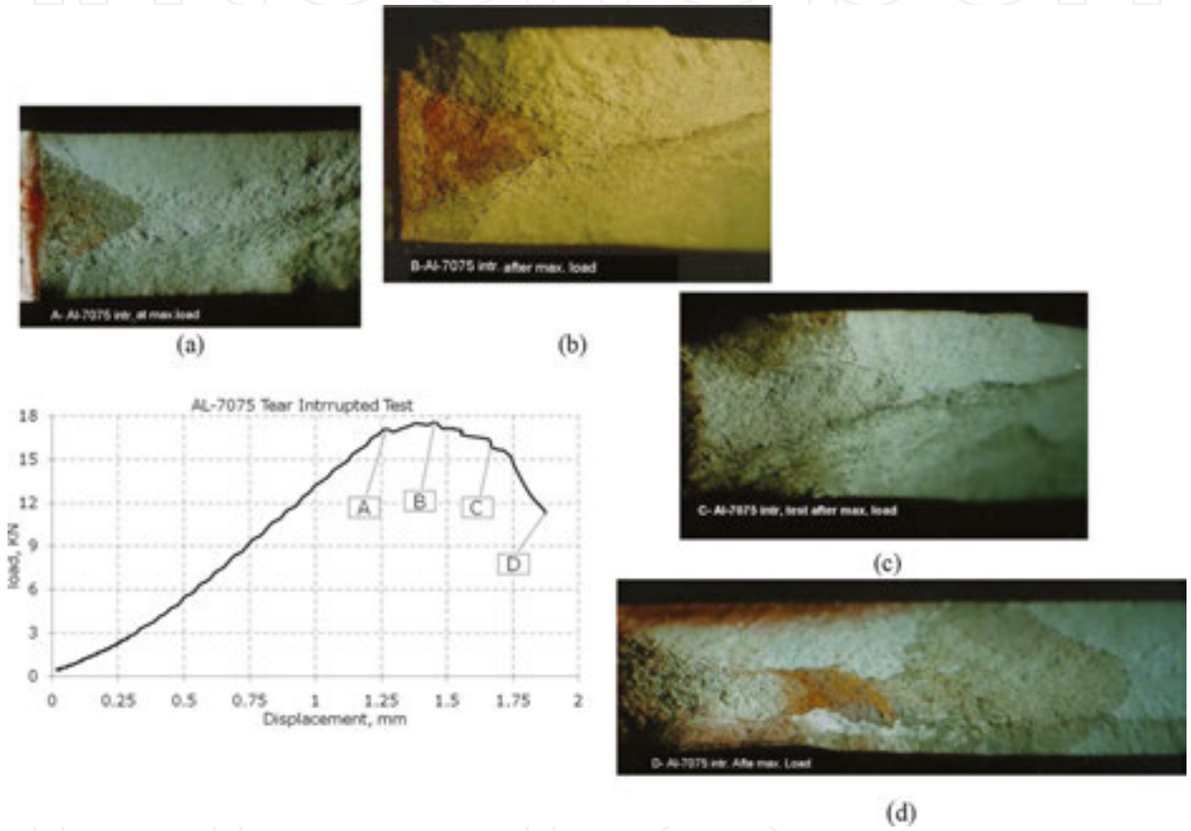

Figure 11. Load-displacement curve for interrupted tear tests performed on AA7075 and related fracture surfaces (a–d) after ink penetration and reloading.

For crack route detection during failure process, the interrupted tear tests were performed on AA7075. In **Figure 11**, the interrupted tear test points and the successive positions of the crack front after penetration of ink into the crack areas are presented. The points A and B correspond to crack initiation and maximum load conditions, respectively. The points C and D show the situations where the load exceeds the maximum value and crack length is equal to or more than half of the specimen net width. **Figure 12** shows load-displacement curves exactly at the test interruption points. At the right side of these curves, the specimens' reloading curves for full failure purpose, after interruption and ink penetration, are presented.

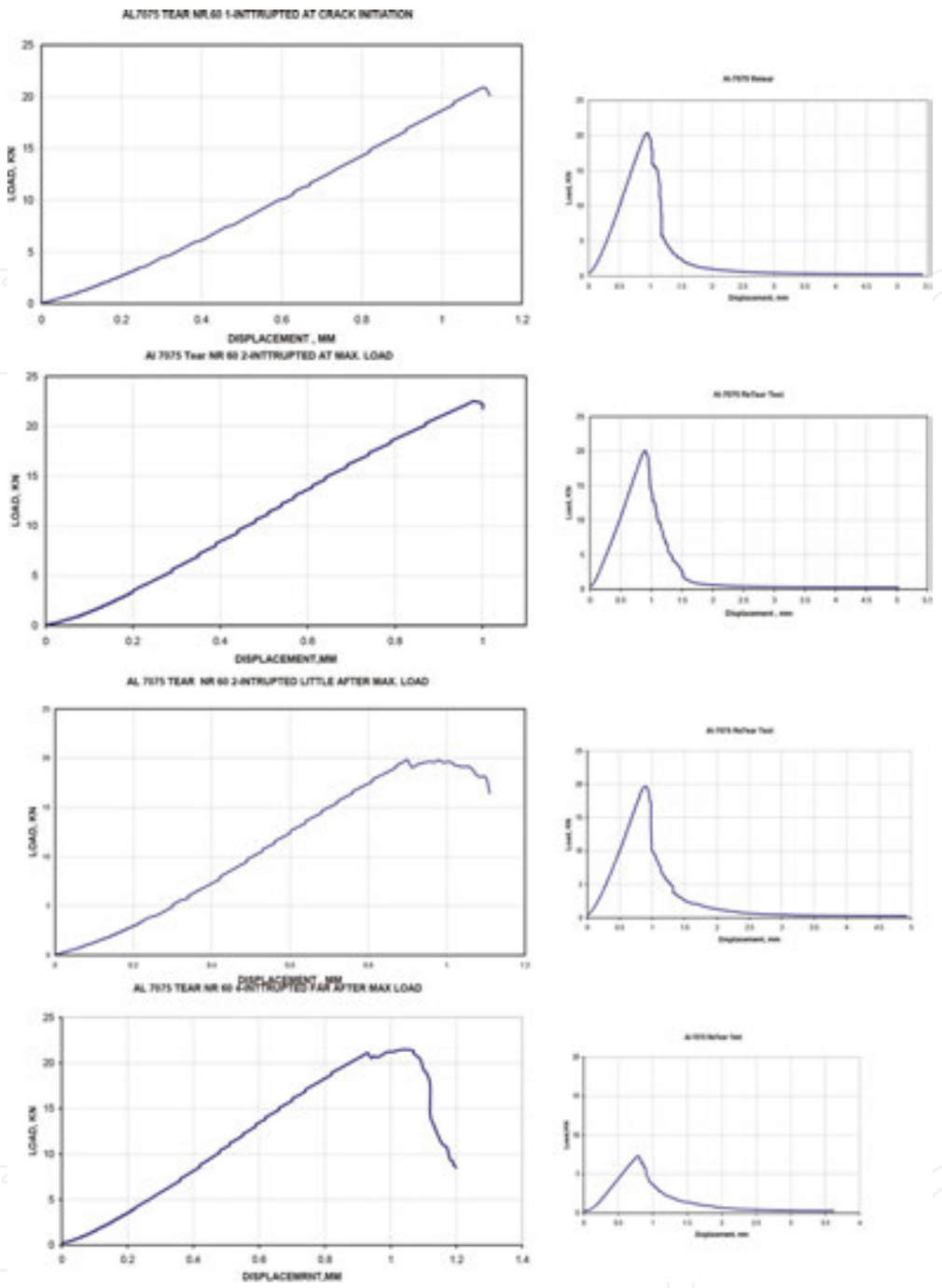

Figure 12. Load-displacement curves for interrupted tear tests at points A–D (left) and reloading curves for full failure purpose (right).

In resultant macrographs of interrupted tear tests, a small triangular zone having its base on the notch root and its normal parallel to the loading direction can be seen, **Figure 11a** and **b**. This area can be considered as failure initiation zone at the notch root. After load increase and reaching the maximum value, it has been reached almost both sides of the specimen. Moreover, the phenomenon called "tunneling", in which the crack front in the middle of flat region advances more than lateral zones, is also evident in these micrographs. As mentioned by Born

http://dx.doi.org/10.5772/64463

et al. [7], at this stage, the crack length is bigger in the middle of the specimen. The slanted zone can be also seen out of the triangle area, **Figure 11c** and **d**. Referring to Bron et al. [7], in thin specimen and presence of plane stress condition, after maximum load only slanted fracture could exist. Nevertheless, in the present study, as mentioned previously, the thickness of samples equals to 6.35 mm which implies that plane strain condition is prevailing. Thus, after maximum load, the triangle zone is followed by lateral slanted zones (sides) and rough flat (central part) zone, see **Figure 11c** and **d**. The growth of triangular and slanted zones is also evident. Eventually, the whole crack front is slanted and slightly curved.

3.4. Fractography

Figures 13 and **14** show the fracture surfaces of tension test specimens. These fractographs indicate that the void nucleation, growth and coalescence are dominant mechanisms in the fracture of specimens. The fracture surfaces in both alloys are mainly covered with dimples which appear around particles. Considering the higher magnification of micrograph in **Figure 14a** comparing to **Figure 13a**, the size of dimples is different in two alloys, being smaller in the case of AA7075. In some parts of fracture surfaces, smooth areas without any dimple are visible, **Figures 13b** and **14b**. This is attributed to the friction during rupture process, which has been also mentioned in other articles [7, 15, 49]. It should be noted that the fracture surface in macroscopic scale was inclined at 45° to the loading direction.

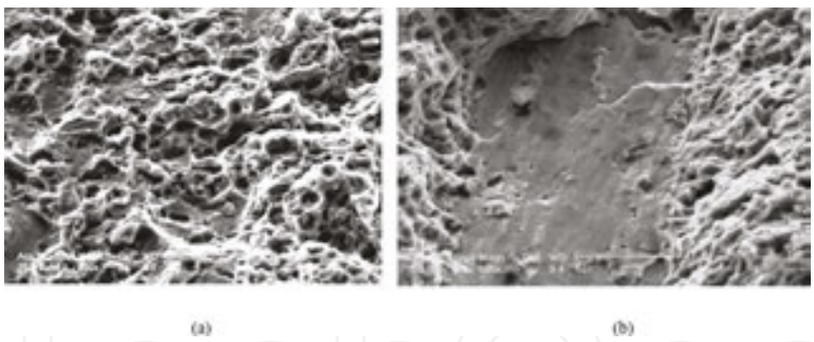

Figure 13. The fractographs of AA7050 tension test specimens illustrating (a) dimple covered area and (b) flat area.

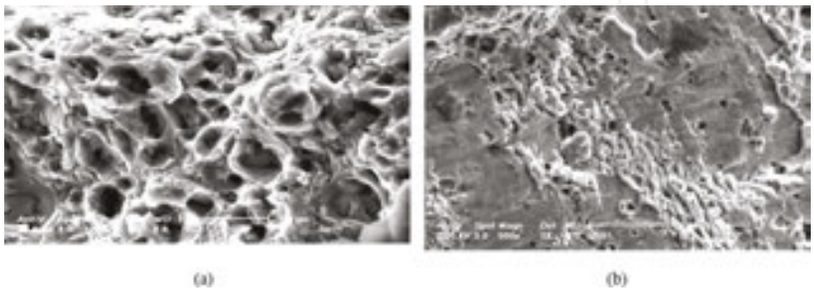

Figure 14. The fractographs of AA7075 tension test specimens illustrating (a) dimple covered area and (b) flat area.

In **Figures 15** and **16**, the fracture surface appearance of type "A" tear test specimens is shown for both alloys. It should be noted that in the flat triangle (dimpled) area, the void formation and void coalescence around second-phase particles are dominant. The diameter of the dimples is slightly bigger than that of the particles which indicates on the void growth after nucleation. On the fractograph of AA7050, the smooth areas representing intergranular fracture are also evident. This mechanism is mainly reported in underaged materials in which low-strength precipitates are seen and there is a high possibility of particles shearing [15, 26]. The sharp V-notch, with low NRR, in type "A" specimens acts as stress concentrator which leads to stress triaxiality condition. In the presence of stress triaxiality, applied stress on the voids operates in three dimensions, which accordingly leads to enhancement of void growth and void coalescence named as "internal necking mechanism" [7, 49]. On this account, the decrease of NRR results in the decrease of alloy's resistance to rupture. On the other hand, the change in rupture mechanism and occurrence of flat areas can cause the dissipation of energy in the specimen and increase in the material's resistance to rupture [49]. At low stress triaxiality ratio, voids tend to coalesce rapidly according to a "void sheet mechanism" which creates smaller dimples in the intervoid ligaments in slanted area, see **Figures 15b** and **16b**.

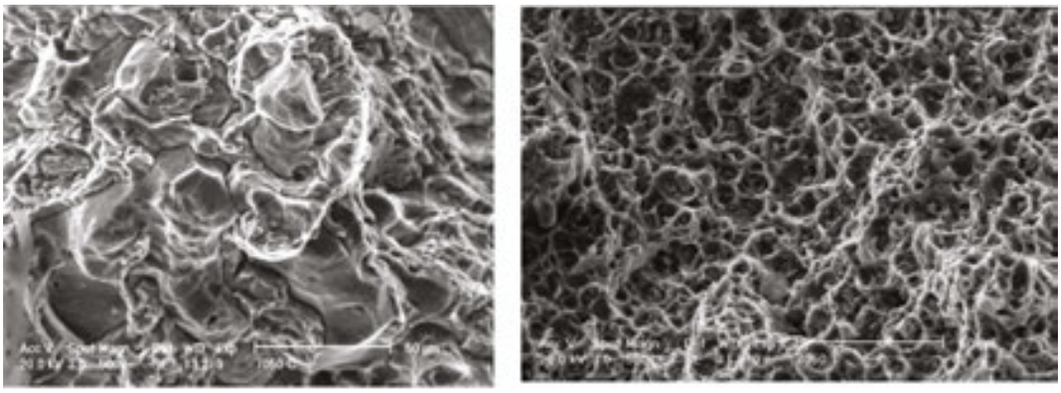

Figure 15. SEM fractographs of type "A" tear specimens for AA7050: (a) flat triangular area and (b) slanted area.

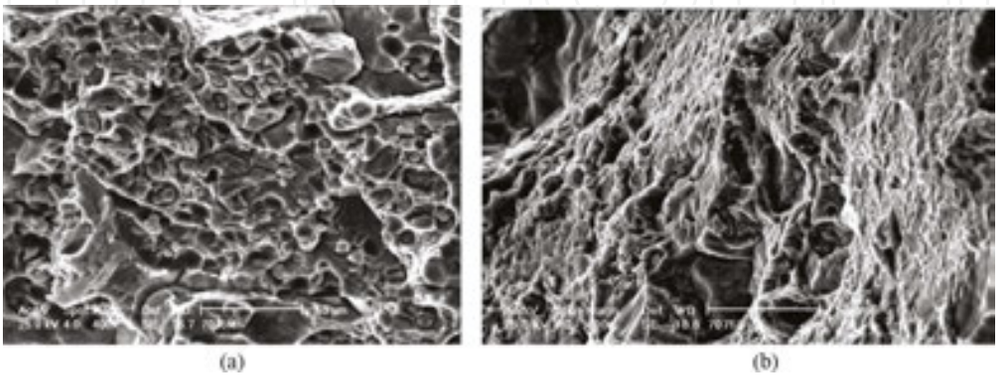

Figure 16. SEM fractographs of type "A" tear specimens for AA7075: (a) flat triangular area and (b) slanted area.

http://dx.doi.org/10.5772/64463

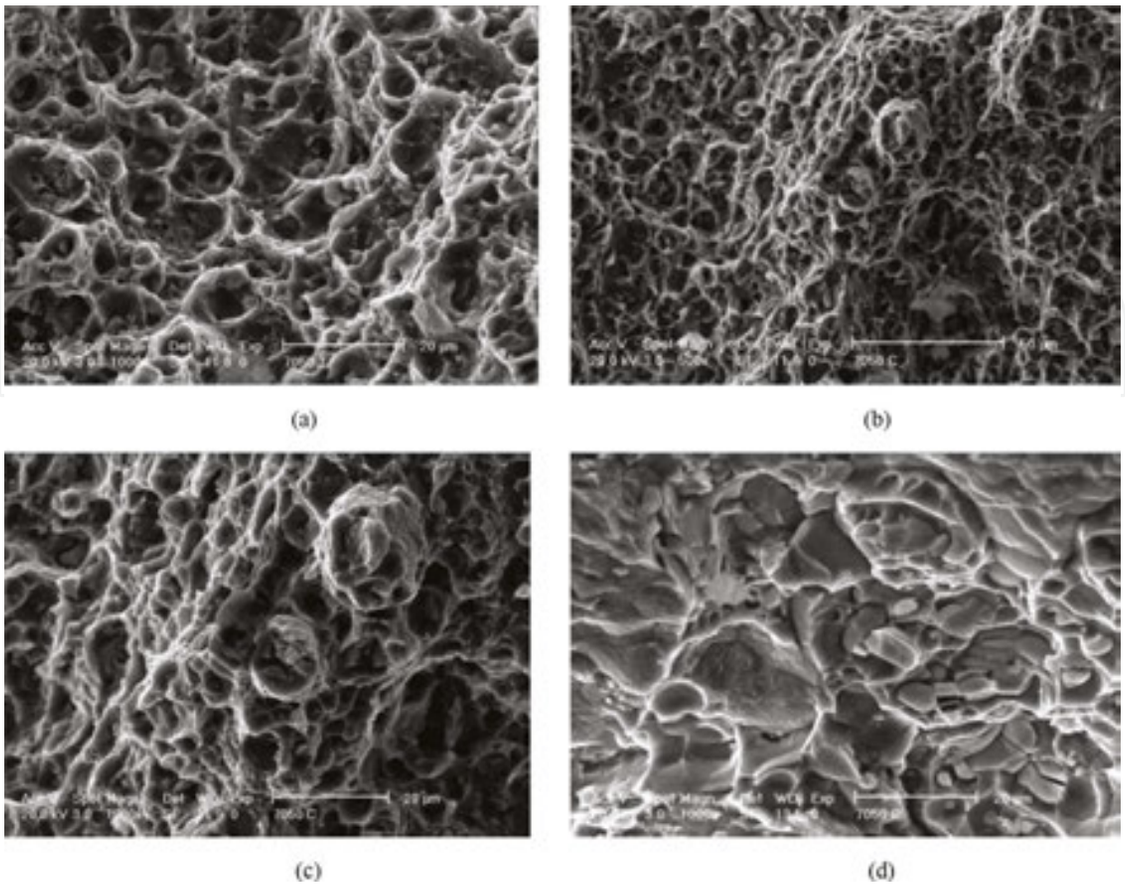

Figure 17. SEM fractographs of type "B" tear specimens for AA7050: (a) flat triangular area, (b) and (c) slanted area and (d) flat area (far from notch root).

In **Figures 17** and **18**, the fractographs of type "B" tear specimens are shown for both alloys. In flat triangle area, the growth of voids is contributed significantly to material rupture. As can be seen in related fractographs, large dimples are present around intermetallic particles. The chemical composition of these particles is cited in previous parts. The most particles in front of the notch are damaged in the first stages of plasticity, see **Figures 17a** and **18a**. The size of dimples observed in triangular area is less than 10 μm in AA7050 and more than 10 μm in AA7075. The slight difference is due to the alteration in the precipitate size and density. The growth of primary dimples will be prevented as it needs high amount of energy. Therefore, after a certain limit, the secondary voids would nucleate around smaller particles. The size of secondary dimples is about 1 μm in both alloys which corresponds to the size of dispersoids. In slanted zone, the "void sheet mechanism" has significant influence on the material rupture and consequently the size of dimples is smaller than triangular area. In flat area, outside the triangular area, almost the same rupture mechanism alike triangular zone is detected. However, in addition to nucleation and growth of voids, decohesion of coarse particles can be observed, see **Figures 17d** and **18d**. Therefore, fractographs prove two major failure micro-mechanisms. Primary voids are first initiated at intermetallic particles. In flat triangle area, i.e., near the notch root, void growth is promoted and rupture is caused by "internal necking" due to void coalescence. In slanted regions these voids tend to coalesce rapidly according to a "void

sheet mechanism" which leads to the formation of smaller secondary voids at dispersoids like (Al_3Zr) in the ligaments between the primary voids.

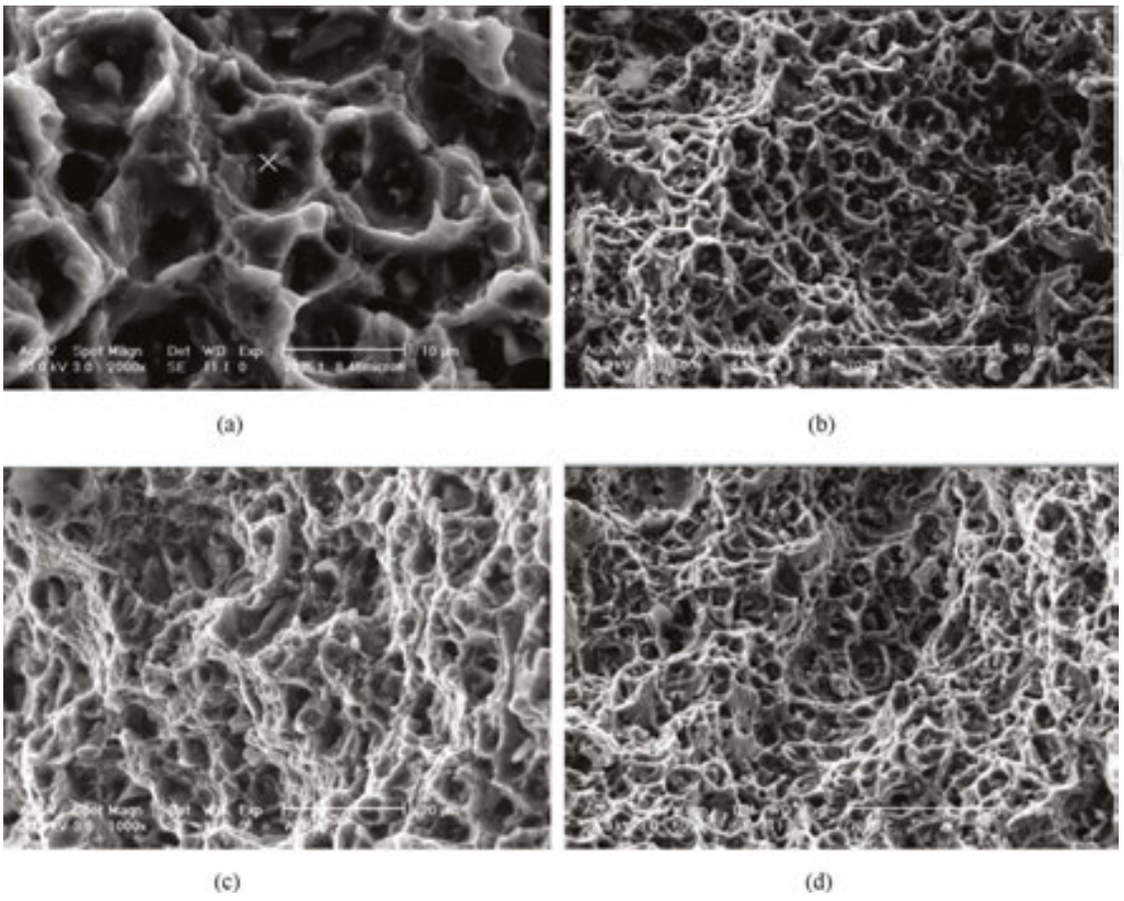

Figure 18. SEM fractographs of type "B" tear specimens for AA7075: (a) and (b) flat triangular area, (c) slanted area and (d) flat area (far from notch root).

4. Conclusions

The following conclusions can be made from the results of this investigation:

- The tear test provides an incredibly valuable variety of information as notch toughness (tear strength to yield strength ratio), crack initiation and propagation energies and notch resistance as unit crack-initiation (UIE) and -propagation (UPE) energies.
- The intermetallic particles act as void nucleation and damage initiation sites.
- The amount, size and distribution of intermetallic particles have been identified as the important factors on failure of the examined alloys.
- Both examined alloys show same damage initiation mechanism, however, the failure mechanism is different in some extent.

- In tear specimen, failure initiates at the notch root in a flat triangular zone perpendicular to the loading direction.
- Depending to the stress condition, two major failure micro-mechanisms i.e. ″internal necking mechanism″ and ″void sheet mechanism″ are prevailing for both alloys.

Author details

Parvin Abachi[1*], Pouyan Shoushtari Zadeh Naseri[2], Kazem Purazrang[3] and Tom W. Coyle[4]

*Address all correspondence to: abapar1056@gmail.com; p.abachi@utoronto.ca

1 Center for Advanced Coating Technologies, Department of Materials Science and Engineering, University of Toronto, Toronto, Canada

2 Faculty of Engineering and Information Sciences (EIS), University of Wollongong, New South Wales, Australia

3 Department of Materials Science and Engineering, Sharif University of Technology, Tehran, Iran

4 Center for Advanced Coating Technologies, Department of Materials Science and Engineering, University of Toronto, Toronto, Canada

References

[1] Starke E.A., Jr., Staley J.T. Application of modern aluminum alloys to aircraft. Prog. Aerospace Sci. 1996;32:131–172. DOI:10.1016/0376-0421(95)00004-6.

[2] Jeong D.Y., Orringer O., Sill G.C. Strain energy density approach to stable crack extension under net section yielding of aircraft fuselage. Theor. Appl. Fract. Mech. 1995;22:127–137. DOI:10.1016/0167-8442(94)00053-4.

[3] Nakai M., Eto T. New aspects of development of high strength aluminum alloys for aerospace applications. Mater. Sci. Eng. A. 2000;285:62–68. DOI: 10.1016/S0921-5093(00)00667-5.

[4] Huda Z., Edi P. Materials selection in design of structures and engines of supersonic aircrafts: a review. Mater. Des. 2013;46:552–560. http://dx.doi.org/10.1016/j.matdes.2012.10.001.

[5] Andreatta F. Local electrochemical behaviour of 7xxx aluminum alloys [thesis]. Netherland: Technische Universiteit Delft; 2004. Pasmans Offsetdrukkerij, Den Haag. ISBN 90-77172-08-4.

[6] Wanhill R.J.H., Schra L., Van Leeuwen H.P.. Some engineering property comparisons for 7050 and AZ 74.61 die forgings. Eng. Frac. Mech. 1979;11:507–524. DOI: 10.1016/0013-7944(79)90075-4.

[7] Bron F., Besson J., Pineau A. Ductile rupture in thin sheets of two grades of 2024 aluminum alloys. Mater. Sci. Eng. A. 2004;380:356–364. DOI:10.1016/j.msea. 2004.04.00.

[8] Smith B. The Boeing 777. Adv. Mater. Process. 2003;6:41–44.

[9] John H.B.I. Application of average stress criterion to fracture of aluminum alloys used in aerospace applications. Arabian J. Sci. Eng. 2013;39:1409–1415. DOI 10.1007/ s13369-013-0669-z.

[10] ASTM E 561-86. Standard practice for R-Curve determination. Annual Book of ASTM Standard. 1993;03.01:577–586. Last previous edition approved in 2015 as E561-15. DOI: 10.1520/E0561-15A.

[11] ASTM B 646-12. Standard practice for fracture toughness testing of aluminum alloys. Annual Book of ASTM Standard. 2012;02.02:1–5. DOI:10.1520/B0646-12.

[12] Kang S., Grant N.G. Notch tensile testing as a measure of the toughness of aluminum alloys. Mater. Sci. Eng. A. 1985;72:155–162. DOI:10.1016/0025-5416(85)90154-5.

[13] Zhu H., Kumai S., Sato A. Tear toughness evaluation of aluminum alloy castings using a small-size specimen. Mater. Forum. 2004;28:1160–1166. DOI: http://doi.org/10.2320/ matertrans.45.1714.

[14] ASTM, B871-01. Standard test method for tear testing of aluminum alloy products. Annual Book of ASTM Standard. 2013;02.02:1–7. DOI:10.1520/B0871-01R13.

[15] Dumont D., Deschamps A., Bréchet Y. A model for predicting fracture mode and toughness in 7000 Series aluminium alloys. Acta Mater. 2004;52:2529–2540. DOI: 10.1016/j.actamat.2004.01.044.

[16] Xie F., Yanb X., Ding L., Zhang F., Chen S., Chu M.G., Chang Y.A. A study of microstructure and microsegregation of Al 7050 alloy. Mater. Sci. Eng. A. 2003;355:144–153. DOI:10.1016/S0921-5093(03)00056-X.

[17] Salmci E. Ageing behaviour of spray Cast Al-Zn-Mg-Cu alloys. Turkish J. of Eng. and Environment Sci. 2001;25:681–686. DOI:5000025193-5000038363-1-PB.

[18] Engdahl T., Hansen V., Warren P.J., Stiller K. Investigation of fine scale precipitates in Al–Zn–Mg alloys after various heat treatments. Mater. Sci. Eng. A 2002;327:59–64. DOI: 10.1016/S0921-5093 (01)01876-7.

[19] Hansen V., Karlsen O.B., Langsrud Y., Gjonnes. Precipitates, zones and transitions during aging of Al–Zn–Mg–Zr 7000 series alloy. Mater. Sci. Tech.. 2004;20:185–193. DOI: 10.1179/026708304 225010424.

[20] Deschamps A., Bréchet Y. Influence of quench and heating rates on the ageing response of an Al–Zn–Mg–(Zr) alloy. Mater. Sci. Eng. A 1998;251:200–207. DOI:10.1016/S0921-5093(98) 00615-7.

[21] Kamp N., Sinclair I., Starnik M.J. Toughness-strength relations in the overaged 7449 Al-based alloy. Metall. Mat. Trans. A. 2002;33:1125–1136. link.springer.com/article/10.1007%2Fs 11661-002-0214-2.

[22] Sauer C., Busongo F., Lutjering G. Influence of precipitation free zones on the test direction dependence of mechanical properties of high strength aluminum alloys. Mat. Sci. Forum. 2002;396–402:1115–1120. DOI:10.4028/www.scientific.net/MSF.396-402.1115.

[23] Clark R., Coughran B., Traina I., Hernandez A., Scheck T., Etuk C., Peters J., Lee E.W., Ogren J., Es-Said O.S. On the correlation of mechanical properties and physical properties of 7075-T6 Al alloy. Eng. Failure Anal. 2005;12:520–526. DOI:10.1016/j.engfailanal.2004.09.005.

[24] Deshpande N.U., Gokhale A.M., Denzer D.K., Liu J. Relationship between fracture toughness, fracture path and microstructure of 7050 aluminum alloy: part I. Quantitative characterization. Metall. and Mat. Trans. A. 1998;29:1191–1201. link.springer.com/article/10.1007% 2Fs11661-998-0246-3.

[25] Oswald L.E. Effects of microstructure on high-cycle fatigue of an Al-Zn-Mg-Cu alloy (Al-7055). [M.Sc. thesis]. University of Pittsburgh, 2003. d-scholarship.pitt.edu/7400/1/oswaldapril2003.pdf.

[26] Dumont D., Deschamps A., Bréchet Y. On the relationship between microstructure, strength and toughness in AA7050 aluminum alloy. Mater. Sci. Eng. A 2003;356:326–336. DOI:10.1016/S0921-5093(03)00145-X.

[27] Srivatsan T.S. An investigation on the cyclic fatigue and fracture behavior of aluminum alloy 7050. Materials Design. 2002;23:141–151. PII: S0261-30690100071-1.

[28] Lumley R.N., Morton A.J., O'Donnell R.G., Polmear I.J. New heat treatments for age-hardenable aluminum alloys. Heat Treating Progress. 2005;3/4:23–29. www.asminternational.org/documents/10192/pdf/ZHTP00502P023.

[29] Dungore P., Agnihotri A. Special heat treatment practices for aerospace aluminum alloys. Heat Treating Progress. 2008;8/3:35–38. http://www.asminternational.org.

[30] Kumar P.V., Reddy G.M., Rao K.S. Microstructure, mechanical and corrosion behavior of high strength AA7075 aluminium alloy friction stir welds – effect of post weld heat treatment. Defence Technol. 2015;11:362–369. http://dx.doi.org/10.1016/j.dt.2015.04.003.

[31] IABG. Bauteilspezifische Werkstoffuntersuchungen, Untersuchungen an Halbzeug 7050-T73651 Bruchzähigkeit und Ermüdungsverhalten. Industrieanlegen Betriebsgesellschaft mbH, IABG, Germany, Bericht Nr. TF-621.3;1976.

[32] Petzow G. Metallographic etching. 2nd edition; ASM International; 1999. 200 p. ISBN: 978-0-87170-633-1.

[33] ASTM B 557M-98. Standard methods of tension testing wrought and cast aluminum- and magnesium-alloy products. Annual Book of ASTM Standard. 1998;02.02:447–457. Current edition approved Oct. 1, 2015. Published October 2015. DOI:10.1520/B0557-15.

[34] Abachi P. Kinetics of crack growth rate in high strength Al-7050 alloy under constant load at 150 °C. [M.Sc. thesis]. Ankara-Turkey: Middle East Technical Uni., 1989

[35] Varli A.E., Gürbüz R. Fatigue crack growth behaviour of 6013 aluminium alloy at different ageing conditions in two orientations. Turkish J. Eng. Environ Sci. 2006;30:381–386.

[36] Sha G., Gerenzo A. Early-stage precipitation in Al-Zn-Mg-Cu alloy (7050). Acta Mater. 2004; 52:4503–4516. DOI:10.1016/j.actamat.2004.06.025.

[37] Chen G.S., Gao M., Wei R.P. Microconstituent-induced pitting corrosion in aluminum alloy 2024-T3. Corrosion 1996;52:8–15. DOI: 10.5006/1.3292099.

[38] Garret G.G., Knott J.F. The influence of compositional and microstructural variations on the mechanism of static fracture in aluminum alloys. Metall. Trans. A. 1978;9:1187–1201. DOI: 10.1007/BF02652242.

[39] Cvijović Z., Rakin M., Vratnica M., Cvijović I. Microstructural dependence of fracture toughness in high-strength 7000 forging alloys. Eng. Frac. Mech. 2008;75:2115–2129. DOI: 10.1016/j.engfracmech. 2007.10.010.

[40] Mackenzie D.S., Totten G.E., editors. Handbook of Aluminum, volume 1: Physical Metallurgy and Processes, Marcel Dekker; 2003. 1310 p.

[41] Su R.M., Qu Y.D., Li R.D., You J.H. Influence of RRA treatment on the microstructure and stress corrosion cracking behaviour of the spray-formed 7075 alloy. Mater. Sci. 2015;51:372–380. DOI: 10.1007/s11003-015-9851-7.

[42] Nasseri P.Sh. The evaluation of notch sensitivity of 7075 & 7050 aluminum alloys and comparison of some mechanical properties. [M.Sc. thesis]. Tehran-Iran: Sharif Uni. of Technology; 2006.

[43] Pao P.S., Gill S.J., Feng C.R., Sankaran K.K. Corrosion fatigue crack growth in friction stir welded Al 7050. Scr. Mater. 2001;45:605–612. DOI:10.1016/S1359-6462(01)01070-3.

[44] Polmear I.J. Light alloys: from traditional alloys to nanocrystalline, 4th edition; Butterworth-Heinemann; 2006. 416 p. ISBN: 0 750663715.

[45] Cai Y., Lang Y., Cao L., Zhang J. Enhanced grain refinement in AA7050 Al alloy by deformation-induced precipitation. Mat. Sci. and Eng. A. 2012;549:100–104. http://dx.doi.org/10.1016/j.msea.2012. 04.011.

[46] Ranganatha R., Kumar V.A., Nandi V.S., Bhat R.R., Muralidhara B.K. Multi-stage heat treatment of aluminum alloy AA7049. Trans. Nonferr. Metals Soc. China 2013;23:1570–1575. DOI:10.1016/S1003-6326(13)62632-1.

[47] Goswami R., Lynch S., Holroyd N.J.H., Knight S.P., Holtz R.L. Evolution of grain boundary precipitates in Al 7075 upon aging and correlation with stress corrosion cracking behavior. Metall. Mat. Trans. A, 2012;44:1268–1278. DOI: 10.1007/s11661-012-1413-0.

[48] Sarkar J., Kutty T.R.G., Conlon K.T., Wilkinson D.S., Embury J.D., Lloyd D.J. Tensile and bending properties of AA5754 aluminum alloys. Mater. Sci. Eng. A 2001;316:52–59. DOI:10.1016/S0921-5093(01)01226-6.

[49] Asserin-Lebert A., Besson J., Gourgues A.F. Fracture of 6056 aluminum sheet materials: effect of specimen thickness and hardening behavior on strain localization and toughness. Mater. Sci. Eng. A 2005;395:186–194. DOI:10.1016/j.msea.2004.12.018.

IntechOpen